

Atmospheric Helium Abundances in the Giant Planets

Nadine Nettelmann^{1,2,3*}, Marina Cano Amoros³, Nicola Tosi³,
Ravit Helled¹, Jonathan J. Fortney²

^{1*}Institute for Computational Science, University of Zurich (UZH),
Winterthurerstr. 190, Zurich, 8057, Switzerland.

²Department of Astronomy and Astrophysics, University of California
(UCSC), High St 1156, Santa Cruz, 95064, CA, USA.

³Institute of Planetary Research, German Aerospace Center (DLR),
Rutherfordstr. 2, Berlin, 12489, Germany.

*Corresponding author(s). E-mail(s): nadine.nettelmann@gmx.de;

Abstract

Noble gases are accreted to the giant planets as part of the gas component of the planet-forming disk. While heavier noble gases can separate from the evolution of the hydrogen-rich gas, helium is thought to remain at the protosolar H/He ratio $Y_{\text{proto}} \sim 0.27\text{--}0.28$. However, spacecraft observations revealed a depletion in helium in the atmospheres of Jupiter, Saturn, and Uranus. For the gas giants, this is commonly seen as indication of H/He phase separation at greater depths. Here, we apply predictions of the H/He phase diagram and three H/He-EOS to compute the atmospheric helium mass abundance Y_{atm} as a result of H/He phase separation.

We obtain a strong depletion $Y_{\text{atm}} < 0.1$ for the ice giants if they are adiabatic. Introducing a thermal boundary layer at the Z-poor/Z-rich compositional transition with a temperature increase of up to a few 1000 K, we obtain a weak depletion in Uranus as observed. Our results suggest dissimilar internal structures between Uranus and Neptune. An accurate in-situ determination of their atmospheric He/H ratio would help to constrain their internal structures. This is even more true for Saturn, where we find that any considered H/He phase diagram and H/He-EOS would be consistent with any observed value. However, some H/He-EOS and phase diagram combinations applied to both Jupiter and Saturn require an outer stably-stratified layer at least in one of them.

Keywords: Giant planets, Solar system, Space missions

1 Introduction

Many planets the size of the ice giants Uranus and Neptune have been detected. However, Uranus and Neptune are the only known planets with deep hydrogen-helium atmospheres that are rich in volatiles and cold enough for processes like condensation and phase separation to occur. On Uranus and Neptune we can study how such processes influence the atmospheric composition, interior structure, and thermal evolution.

As the two remote ice giants Uranus and Neptune have the coldest tropospheres and perhaps also the coldest interiors of any known orbiting planet, one may consider them as end-members in the planetary landscape. However, they may unify a number of important planet properties and therefore be of central importance for our understanding of the diverse population of planets.

One such important property may be H/He phase separation. The weakly irradiated gas giant Jupiter is partially shaped by the phase separation of hydrogen and helium as indicated by its atmospheric helium depletion (Niemann et al, 1998; von Zahn et al, 1998). If the gaseous H/He-component is present in the deep interiors of Uranus and Neptune, H/He phase separation may also occur there, but has not been studied in print for the ice giants before.

The landscape is further populated by strongly irradiated hot Jupiters and warm Neptunes. Their close orbits suggest that they formed farther out and migrated inward by disk-planet interaction. For Uranus and Neptune, the Nice model of Solar System formation suggests that the ice giants formed closer to the Sun and migrated away later by interaction with a disk of planetesimals (Tsiganis et al, 2005). Therefore it is possible that the formation locations of warm Neptunes and Uranus and Neptune are not that different. From accurately measured planet masses (M_p) and radii (R_p) a bulk heavy element enrichment of extrasolar giant planets that increases toward lower-mass planets has been inferred (Thorngren et al, 2016) under the assumption of adiabatic interiors. With at least 65% of their mass in heavy elements, Uranus and Neptune fit well in the exoplanet M_p - Z_p relation, where Z_p is a planet's heavy element mass fraction. Thus it could also be that planets of that mass and size share similar bulk heavy element enrichment wherever they formed.

Within current observational uncertainties, Uranus and Neptune are extraordinarily similar to each other in atmospheric composition, gravity, magnetic field, rotation rate, and atmospheric temperature. These constraints are not available for exoplanets, however, one may assume that an exo-equivalent to Uranus and Neptune by mass and radius shares a similar structure. It is therefore important to identify which structure properties they may have in common and which may be influenced by the thermal profile and evolution, as those will differ with the different irradiation levels they receive.

The most commonly found type of planets has even lower masses of 5–10 M_E , compared to the 14.5 M_E and 17.2 M_E of Uranus and Neptune. These so-called sub-Neptunes in the 2–3 R_E radius range occur at an average rate in the Galaxy of ~ 0.5 planets per Sun-like star with a factor of ~ 2 uncertainty (Hsu et al, 2019; Kunimoto and Matthews, 2020). Whether sub-Neptunes are mostly made of volatiles or of rocks

with an extended gaseous atmosphere is one of the fundamental questions in planetary science and clearly not to be resolved with further M_p - R_p measurements alone. The same major question applies to Uranus and Neptune. Knowledge of bulk- Z , the ice:rock ratio, and the interior Z -distribution yields information on the location of formation and the conditions in the planet-forming disk. As an advantage over exoplanets, tracing the motion of satellites around Uranus and Neptune has allowed us to place constraints on their interior Z -distribution through the density distributions that fit the gravity field measurements (Nettelmann et al, 2013; Movshovitz and Fortney, 2022; Neuenschwander and Helled, 2022).

Interior models of Uranus and Neptune constrained by the gravity data require a H/He-rich atmosphere and a high- Z deep interior, but gravitational harmonics measurements do not allow us to distinguish between a more rocky or a more icy deep interior, nor to determine whether the transition is sharp or gradual (Helled et al, 2020). Depending on the temperature profile and the assumed ice:rock ratio, up to 24% H-He could exist in their deep interiors (Helled et al, 2011; Nettelmann et al, 2013). Thus as in Jupiter, H/He-demixing could occur there and influence the observable atmospheric composition.

Direct measurements of element abundances are needed to place additional constraints. However, condensible volatiles are not necessarily well mixed even deep in the troposphere. As revealed by the Juno Orbiter, Jupiter’s ammonia abundance remains variable even down to ~ 30 bars, which is well below the ammonia cloud level (Guillot et al, 2020).

Fortunately, noble gases like helium are thought to be well-mixed in the troposphere. Unfortunately the mass spectrometer aboard the Cassini spacecraft stopped working before the troposphere of Saturn was reached. So far, the only accurate noble gas abundance measurements in a giant planet’s atmosphere are those by the Galileo entry probe at Jupiter (Atreya et al, 2003). This in-situ measurement has been and still is highly valuable for our learning process about Jupiter’s interior structure and evolution as well as the behavior of hydrogen and helium at high pressures. The entry probe measured a higher He abundance than inferred from the previous Voyager occultation and remote sensing data. This makes the Voyager values for Saturn (Conrath and Gautier, 2000) and the ice giants questionable.

In this work we address the helium abundance in the atmospheres of the giant planets in the Solar System. We consider the possibility that the atmospheric He abundances in Uranus and Neptune differ from the *final* Voyager values, which are at a protosolar level for Uranus and an enhanced level for Neptune (Atreya et al, 2020). We assume that H/He exists in their deep interiors, where it can undergo phase separation and influence the He abundance above in the molecular-hydrogen region (Stevenson and Salpeter, 1977b,a). We thus aim to predict the atmospheric helium abundance as a result of H/He phase separation, but we also caution that our interior model assumptions may be too simplistic and that an inversion from a future He abundance measurement to internal structure will be non-unique. Yet, different structure models will reflect on a variety of observational parameters. Should an optimization effort be conducted about which parameters should be measured in order to rule-out certain

models, this work aims to make the point that the atmospheric helium abundance be part of the study.

In Section 2 we describe the three H/He phase diagrams that we use to calculate the equilibrium He abundance after phase separation (2.1), the interior model assumptions (2.2), and the three Equations of State (EOS) that we use to compute planetary temperature-pressure (P - T) profiles (2.3). In Section 3 we review the observational He/H abundance measurements. Section 4 presents the results for the atmospheric He abundances. In Section 5 we discuss what a putative atmospheric probe measurement might imply for the internal structure of the outer planets. Our main points are summarized in Section 6. In Appendix A we describe the construction of the BLM21-N23 phase diagram.

2 Methods

2.1 H/He phase diagram

We apply three H/He phase diagrams. Among them are the two published H/He phase diagrams that provide the demixing temperature $T_{\text{dmx}}(P; x_{\text{He}})$ as a function of pressure P and on a dense grid of He particle concentrations $x_{\text{He}} = N_{\text{He}}/(N_{\text{He}} + N_{\text{H}})$ (Lorenzen et al, 2009, 2011; Schöttler and Redmer, 2018). Hereafter, they are referred to as LHR0911 and SR18, respectively. The third H/He phase diagram is derived from the experimental data of (Brygoo et al, 2021). Our construction thereof is described in Appendix A and it is referred to as BLM21-N23.

The helium mass fraction is obtained as $Y = 4x_{\text{He}}/(1 + 3x_{\text{He}})$. We assume that water, if present, is fully dissociated and contributes two H atoms per H_2O molecule. This upper limit to the number of H atoms applies if water is in the plasma phase, which occurs at typical H/He demixing pressures of 1–2 Mbar for temperatures $T \gtrsim 5000$ K (Redmer et al, 2011). The adiabats of Uranus and Neptune run close to the super-ionic/plasma phase transition. If the interior is warmer than along an adiabat the deep adiabats could indeed pass through the plasma phase.

The LHR0911 H/He phase diagram is obtained from DFT-MD simulations of H-He systems. Depending on the P - T conditions chosen, phase separation into a He-rich phase and a He-poor phase can directly be seen in the simulation box. However, this phenomenon occurs in the simulation only if the number of particles in the box, which has periodic boundary conditions, is sufficiently high. For example, Lorenzen et al (2011) observe demixing in their simulation at 6000 K and 24 Mbar when using a high number of electrons like 2048. Chang et al (2023) use a machine-learning approach to directly simulate H/He demixing in even larger systems of up to 27,000 particles. Unfortunately, the direct simulation of demixing is computationally highly demanding. Therefore, the common method of choice is to simulate a mixed H-He system with much fewer particles where the then stronger thermal fluctuations may prevent the system from adopting a more ordered demixed state. Lorenzen et al (2011) and Schöttler and Redmer (2018) run their simulations for the complete H/He demixing diagram with 64 electrons.

Preference for mixing or demixing and the two equilibrium He-concentrations in the latter case are then determined according to the thermodynamics criterium that

a system will strive to reach a state of minimum Gibbs free energy $G(x; P, T) = U(x) + PV(x) - TS(x)$. This free energy is related to the enthalpy H via $G = H - TS$. Its differential reads $dG(x) = V(x)dP - S(x)dT$, or $dG(x) = dH(x) - S(x)dT - TdS(x)$.

In practice, the energy difference ΔG between the assumed mixed state $G(x)$ and the superposition of the fully demixed states, $xG(0) + (1-x)G(1)$ is calculated at a given temperature T and pressure P . If the Gibbs free energy of mixing $\Delta G(x)$ shows two minima, this is interpreted as preference for demixing and a double-tangent construction is applied to determine the equilibrium abundances x_A on the He-poor side and x_B on the He-rich side. To determine the minima and the double-tangent accurately, a Redlich-Kister Fit is applied to $G(x; P, T)$ at every P, T point (Lorenzen et al, 2009; Schöttler and Redmer, 2018).

At constant temperature, $-d(TS)$ reduces to $-TdS$. The entropy of the mixed state is $S(x) = xS(0) + (1-x)S(1) + S_{\text{mix}}$. In the difference ΔS between the assumed mixed state $S(x)$ and the superposition of the fully demixed states, the first two terms cancel so that only the entropy of mixing S_{mix} survives. ΔG at constant temperature can thus be calculated as $\Delta G(x) = \Delta H(x) - T\Delta S_{\text{mix}}(x)$. The enthalpy $H(x; S, P) = U(x) + PV(x)$ is obtained from the thermal EOS $P(x; V, T)$ and the internal energy $U(x; V, T)$. Both $U(T, V)$ and $P(T, V)$ are readily accessible from the DFT-MD simulations but depend on the exchange-correlational functional chosen. The choice of the exchange-correlational functional and the approximation used for S_{mix} therefore matters.

Using the ideal entropy of mixing is the simplest approach as it neglects interparticle interactions. A more sophisticated method has been elaborated for H-He mixtures. Morales et al (2013) perform thermodynamic integration to relate calculated entropy to well-known cases at less extreme P - T conditions via the coupling-constant integration method. This approach was also adopted for the SR18 diagram. While the difference between both approaches is negligible for He-particle concentrations up to 0.2 (McMahon et al, 2012), to be compared to the protosolar value $x_{\text{He}} = 0.086$, the non-ideal contributions strongly influence the Gibbs free energy of mixing at high He concentrations and thus the presence and location of minima (McMahon et al, 2012).

H/He demixing is thought to be driven by the metallization of hydrogen. For a detailed review of investigation of hydrogen metallization and in the presence of helium, see McMahon et al (2012). The vdw-DF1 functional yields metallization pressure at ~ 2 Mbars. This is in good agreement with the dynamic compression experiments performed at the National Ignition Facility using laser energy to near-isentropically compress D samples (Celliers et al, 2018). In these experiments, the insulator-to-metal transition is taken to be a region of steepest slope in the measured reflectivity. A value of 2 Mbar goes in the direction of the 3 Mbar inferred from a jump in reflectivity observed upon compression of multiply shocked D samples using the Z-machine at the Sandia National Laboratory (Knudson and Desjarlais, 2017). The vdw-DF1 functional yields a slightly stiffer Hugoniot than the PBE functional in better agreement with the early gas gun data (Knudson et al, 2015).

A third series of experiments used laser-heated diamond-anvil-cells (DAC) to compress hydrogen. Here, a first-order insulator-metal transition is seen at 1-1.7 Mbar in agreement with the DFT-MD simulations when using the PBE functional (Zaghoo et al, 2016). These experiments also reproduce the maximum compression ratio of 4.5

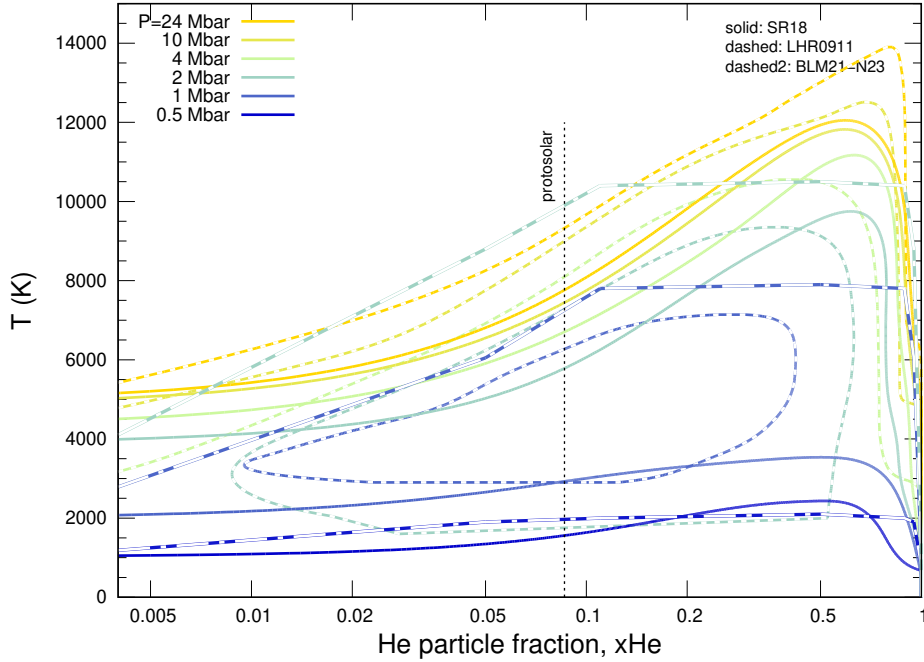


Fig. 1 The phase diagrams of LHR0911 (dashed) and SR18 (solid), and our version of BLM21 (dashed2) for 0.6, 1, 2 Mbars. The vertical dotted black line highlights the protosolar He/H ratio. Color codes isobars as labeled.

at 50 GPa along the principal Hugoniot as measured at the Z-machine (Knudson et al, 2015). However, the PBE-functional based Hugoniot maintains a rather high compressibility toward lower pressures at 30-40 GPa where the experimental data (gas gun, Z-machine) suggest a stiffer EOS. For reviews of recent work on hydrogen metallization and in particular under giant planet conditions we refer the reader to Goncharov (2020) and Helled et al (2020). To summarize, the LHR0911 data set uses the PBE functional and ideal entropy of mixing. The (Morales et al, 2013) data set is built on the PBE functional and the entropy of mixing including interaction effects (non-ideal entropy of mixing). SR18 use the vdw-DF1 functional and non-ideal entropy of mixing.

In Figure 1 we compare the three phase diagrams in terms of the demixing temperatures $T_{\text{dmx}}(P; x_{\text{He}})$. As one can see, differences in T_{dmx} between LHR0911 and SR18 easily amount to 1000–1500 K, with the LHR0911 model yielding higher demixing temperatures wherever it predicts demixing at all.

The SR18-based $T(P)$ curve at protosolar abundance (Fig. 2) transitions smoothly into the MonteCarlo simulations results of Schouten et al (1991) and further extrapolates well to the DAC experimental result at a few GPa by Loubere et al (1991). Despite its relatively high demixing temperatures, even the LHR0911 data set does not reach a temperature of 10,000 K at 1.5 Mbar but rather of around 6000 K. Such a high temperature value was measured at the drop in the reflectivity, which was interpreted as a sign of crossing the phase boundary in dynamically compressed H/He samples

(Brygoo et al, 2021). On the other hand, temperatures along the phase boundary for $x_{\text{He}} = 0.11$ ($Y=0.33$) used in the experiment fall steeply toward lower pressures. As described in Apx. A, we also assume a steep decrease for lower He-concentrations. As a consequence, the demixing temperature at 1 Mbar and a protosolar He-concentration of our version of the BLM21 data comes close to that of the LHR0911 diagram. Overall, Figure 1 indicates there may be significant uncertainties in the H/He phase diagram.

2.1.1 Equilibrium particle concentration x_A

Suppose there is a parcel of protosolar H/He ratio $x = x_{\text{proto}}$ in the interior of the planet at 2 Mbars and 5000 K. The parcel under these conditions would rain-out He-rich droplets until a concentration of respectively $x_{\text{He}} \sim 0.03$ (LHR0911) or $x_{\text{He}} = 0.06$ (SR18) is reached, see Figure 1. This is the equilibrium concentration x_A on the phase boundary. It can be determined for any P, T -point where $T(P; x) \leq T_{\text{dmx}}(P; x)$.

2.2 Planet interior profiles

We compute interior P - T profiles, not interior models. We assume background interior heavy element abundances Z that span a wide a range guided by previous series' of models for Uranus and Neptune (Helled et al, 2011; Nettelmann et al, 2013, 2016; Scheibe et al, 2021) Saturn (Nettelmann et al, 2013; Ni, 2020; Militzer et al, 2019; Mankovich and Fuller, 2021), and Jupiter (Nettelmann et al, 2021; Miguel et al, 2022; Howard et al, 2023; Militzer and Hubbard, 2023). For the ice giants we consider two cases, an adiabatic case and one with a thermal boundary layer (TBL). The latter, non-adiabatic case is described in Section 2.4.2.

In the adiabatic case, we compute P - T profiles under the assumption that the interior has a classical three-layer structure with an outer, heavy-element-poor envelope of water abundance Z_1 , an inner, water-rich envelope of water abundance Z_2 , and a rocky core. The transition between the envelopes occurs at a transition pressure $P_{1,2}$. If $P_{1,2}$ and the water abundances Z_1, Z_2 are adjusted to yield density distributions that are consistent with the low-order gravitational harmonics J_2, J_4 , one can find for Uranus $8 < P_{1,2} < 20$ GPa, $0.01 < Z_1 < 0.2$, and $0.87 < Z_2 < 0.95$, for Neptune $5 < P_{1,2} < 150$ GPa, $0.01 < Z_1 < 0.65$, and $0.7 < Z_2 < 1$, and for Saturn $P_{1,2} \sim 0.5$ to few Mbars, Z_1 up to a few times solar, Z_2 around Z_1 or up to 0.5 if a deep-seated gradient is allowed for. The situation for Jupiter is unclear because, except for few models based on MH13-H/He-EOS (Militzer and Hubbard, 2023), HG23+MLS22 H/He-EOS (Howard et al, 2023), or CD21 but then with enhanced interior temperatures (Debras and Chabrier, 2019), adiabatic models constrained by the tight Juno gravity data fail to reproduce Jupiter's observed surface temperature. Nevertheless, current Jupiter models share the property of a low outer envelope metallicity of 0 - $2 \times$ solar, Z_2 around Z_1 or slightly enriched up to $Z \simeq 0.2$, and $P_{1,2}$ in the 1-20 Mbar range. Whether the deep interior enrichment in Jupiter occurs gradually or sharply cannot be decided from the gravitational harmonics data alone. The Juno mission has revolutionized the label for a deep region of enhanced- Z . It is now called a *dilute* core (Wahl et al, 2017; Mankovich and Fuller, 2021).

The way the above described models matter for this work is as follows: In Uranus and Neptune, the He rain region is located in the heavy element-rich deep envelope. We vary the water mass fraction $Z_{\text{H}_2\text{O}}$ between 0 (rocky case) and 0.90. In Jupiter, He-rain occurs in the outer, heavy-element poor envelope. In Saturn, the He-rain region reaches across the two envelopes of potentially slightly different but generally low Z . A level $Z \sim 0.1$ near $0.5\text{--}0.6 R_{\text{Sat}}$, i.e. near the top of the demixing region, is required by Saturn models that aim at explaining the $n = 1, l = 2, m = -2$ mode observed in Saturn’s C-ring by a g-mode that is trapped in an extended, inhomogeneous dilute core (Fortney et al, 2023). The dilute core regions of higher- Z values in Jupiter and Saturn are deep enough that they do not matter for the determination of the He abundance at the top of the He-rain region, where Z is still low. The upper limit of the $M_p\text{--}Z_p$ relation derived from exoplanets with measured mass and radius suggest Z up to 0.9 for Saturn-mass planets and Z up to 0.5 for Jupiter mass planets (Thorngren et al, 2016).

For all planets, we assume a constant- Z value along the adiabat that is varied between 0 and 0.9. This Z is water. The Z -value acts as a dilution of the He/H-ratio and it can influence the $P\text{--}T$ profile. If water in the He-rain region is dissociated it contributes two H-atoms per water molecule. This dilutes the He/H-ratio. If the adiabat is cold enough, water could also be in the superionic phase, where two protons are released per H_2O molecule, although if H/He phase separation occurs in a superionic environment is unknown. A low Z -value means that Z can be rocks or that water has a low abundance. We neglect the possibility that, if Uranus and Neptune are rock-rich, the dissociation of Fe-bearing rocks can lead to the absorption of H atoms into Fe-H alloys (Horn et al, 2023). This process would tend to enhance (anti-dilute) the deep He/H ratio. However, we expect the number of H-atoms entering this pathway to be negligible.

Including heavy elements in the computation of the entropy affects the resulting adiabatic $P\text{--}T$ profile when $Z \gtrsim 0.2$ (Baraffe et al, 2008). Volatiles in the entropy computation lead to colder adiabats. For example, the icy Uranus model (Bethkenhagen et al, 2017), with its purely icy interior ($Z_2 = 1$) has low core temperature of only 4000 K compared to the ~ 6000 K of adiabatic Uranus models with a deep H/He-content of ~ 0.1 (Nettelmann et al, 2013). For simplicity however, our $P\text{--}T$ profiles are based solely on the EOS of H and He when using the CMS19 or the CD21 EOS, see Section 2.3.

Given interior abundances in Z and Y , the adiabat is uniquely defined by the 1-bar surface temperature. Current Uranus and Neptune have $T_{1\text{bar}} \sim 75$ K (Lindal, 1992), but we calculate series’ of adiabats where $T_{1\text{bar}}$ starts at high values corresponding to younger or more massive or closer-in planets.

2.3 Equations of state

With the advent of extensive computer simulations an increasing number of H/He-EOS variants has been offered over the past two decades that are in good agreement with results from compression experiments (Desjarlais, 2003). Here, we use three different H/He-EOS: CMS19 (Chabrier et al, 2019), CD21 (Chabrier and Debras, 2021), and REOS.3 (Becker et al, 2014). When $T_{1\text{bar}} < 128$ K, we use H/He-REOS.3 for the outer

region up to 140 K. This choice led to a smoother transition in $Y_{\text{atm}}(T_{1\text{ bar}})$ than a cut at 100 K would. For the Z -component we use H2O-REOS, but only in conjunction with REOS.3.

Both CMS19 and CD21 EOS are convenient to use because they provide tabulated entropy data. CMS19-EOS provide tables for pure H and pure He for temperatures $T \geq 100\text{K}$. These tables can be combined using the linear mixing assumption. This way non-ideal effects on the entropy of mixing between H and He are ignored. The effective H-EOS of the CD21-EOS tables on the other hand does include non-ideal mixing effects. For CD21 EOS and the particular He mass fraction of 0.245, the entropy of the linearly mixed system will be the same as that of the full H-He mixture according to the binary mixture simulations of [Militzer and Hubbard \(2013\)](#). One can therefore expect the resulting $Y_{\text{atm}}-T_{1\text{ bar}}$ -curve of intermediate non-ideal mixtures between $Y = 0$ and 0.245 to fall in between the results for CMS19 and CD21 EOS. [Howard and Guillot \(2023\)](#) have constructed non-ideal entropy corrections for any intermediate mixture. For Jupiter and its observed abundance of 0.238, the influence on interior P - ρ profiles between the corrected version and CD21 EOS is small. The smallness shows up for instance as an only 1 K difference in the 10–20 K shift of the $T_{1\text{ bar}}$ temperatures that would be needed to lift the atmospheric- Z from interior models up to $\sim 1.3\times$ solar in Jupiter. While P - ρ is important for gravity, P - T is important for demixing.

For H/He-REOS, we use our usual procedure of thermodynamic integration to compute adiabats for a given mixture EOS including water. This procedure requires only density and internal energy as a function of (P, T) . In the mixture EOS, water is included by its contribution to both density and internal energy assuming linear mixing. Thus the contribution of the Z -EOS to the ideal entropy of mixing is implicitly included in this case.

Figure 2 shows H/He adiabats and demixing curves in P - T space for the three H/He-EOS and the three H/He-phase diagrams, respectively. All curves are for $Y = 0.27$. The adiabats have either $T_{1\text{ bar}} = 166.1\text{K}$ as measured by the Galileo entry probe in Jupiter, or $T_{1\text{ bar}} = 75\text{ K}$ representative of Uranus and Neptune. While all three phase diagrams suggest that He in the entire deep interior underneath the 1 Mbar level would demix in the ice giants, the predictions for jovian planets are highly sensitive to both the phase diagram and the H/He-EOS. For instance, only the CD21-adiabat is cold enough to touch the SR18 H/He-demixing region within the uncertainty of $\pm 500\text{ K}$ of the latter. The rather warm REOS-adiabat suggests a demixing region in Jupiter between 1 and 4 Mbars for the BLM21-N23 H/He phase diagram, although the bottom pressure could be different if the He-gradient, mass conservation, and super-adiabaticity were taken into account as in ([Nettelmann et al, 2015](#)), or if the demixing curve would flatten less strongly.

2.4 Helium depletion in the planet

At a given $T_{1\text{ bar}}$, the adiabat $T(P; Y)$ is compared to the phase boundary $T_{\text{dmx}}(P; Y)$. When overlap is detected, we can record the pressure range over which demixing occurs; it is bounded by P_{in} and P_{out} . An iterative procedure is employed that lowers Y until the then colder adiabat (the adiabatic gradient increases with Y) only touches

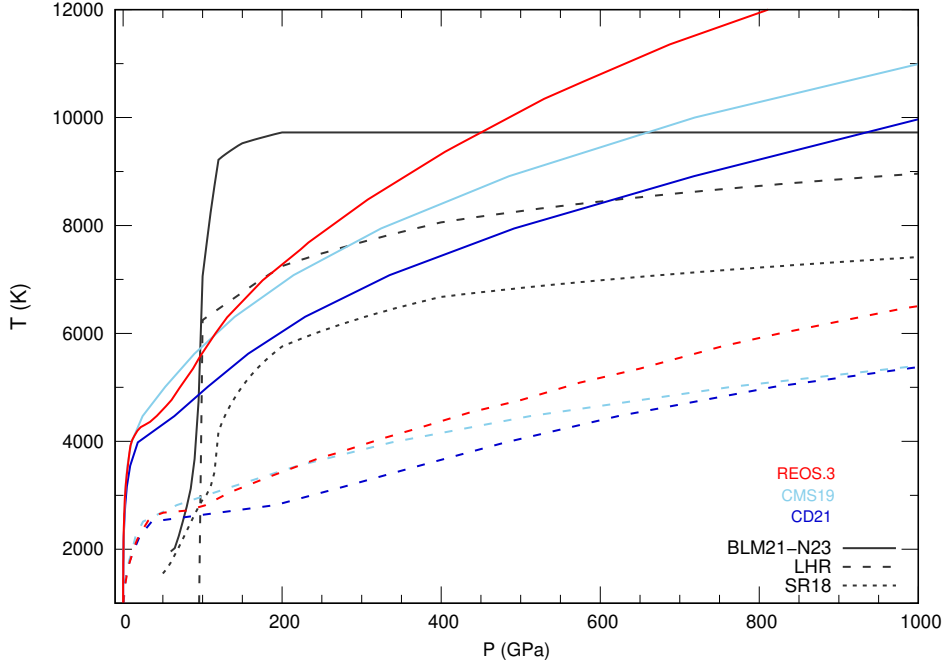


Fig. 2 Demixing curves and adiabats for $Y = 0.27$. Grey lines are the demixing curves for the three H/He phase diagrams (solid: BLM21-N23, dashed: LHR0911, dotted: SR18). Colored lines show the adiabats constrained by $T_{1 \text{ bar}} = 166.1 \text{ K}$ (solid) and $T_{1 \text{ bar}} = 75 \text{ K}$ (dashed) for the three H/He EOSs (red: REOS, blue: CD21, light blue: CMS19).

the H/He phase boundary ($P_{\text{touch}} = P_{\text{in}} = P_{\text{out}}$). With the LHR0911 phase diagram, $P_{\text{touch}} \sim 100 \text{ GPa}$ near the metallization pressure, while with SR18, most solutions have $P_{\text{touch}} \sim 200 \text{ GPa}$, which in turn is characteristic of the metallization pressure in the vdW-DF1-based hydrogen system, see Section 2.1.

This converged new helium abundance Y_A satisfies $T(P_{\text{touch}}; Y_A) = T_{\text{dmx}}(P_{\text{touch}}; Y_A)$. It is the minimum equilibrium abundance. At even lower values $Y < Y_A$ along the adiabat, the system would be miscible. Y_A is the helium mass fraction that is equivalent to the equilibrium particle fraction x_A , see Section 2.1.1.

At deeper levels below P_{touch} , the equilibrium He abundance would increase with depth until either the adiabat leaves the He-rain region at a sub-saturated level (Jupiter case) or the remaining volume becomes too small to dissolve all the rained-out helium and He-layer formation occurs (saturated Saturn case). For the dichotomy between Jupiter’s and Saturn’s internal structure due to He rain, see Mankovich and Fortney (2020). Here we ignore what happens to the deeper interiors.

2.4.1 He depletion in the atmosphere

If convective motions transport a He-poor parcel of concentration x_A upward, it will act to deplete the region above when it dissolves. If convective motions transport a parcel of concentration $x_{\text{He}} > x_A$ downward into the demixing region, it will undergo

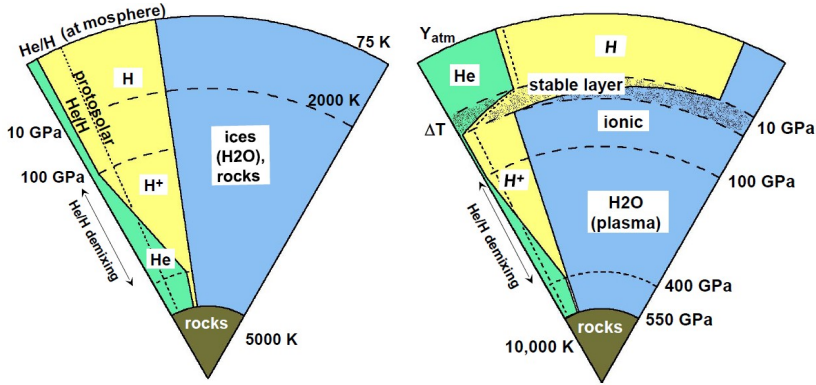


Fig. 3 Schematic 2D interior structure models of a Uranus or Neptune-like ice giant illustrating the mass fractions of hydrogen (yellow), helium (green), and water (blue) over radius (radial linear scale). At the center of the planet is a $\sim 1 M_E$ rocky core. Left: This model assumes that the depletion in He caused by H/He demixing at Mbar pressures extends all the way to the atmosphere due to convection or other means of efficient communication. Due to convection the Z -distribution should be homogeneous, which however is not supported by the gravity data. The dotted line shows a constant protosolar He/H mass ratio of 0.27. Right: A stable layer (shaded) between the ice-poor outer and the ice/rock rich deep interior acts as a thermal boundary layer. It reduces the efficiency of heat and particle transport between the atmosphere and the deep interior. Primordial heat can be trapped inside, resulting in a temperature increment ΔT . In addition, the stabilizing Z -gradient may permit a destabilizing He-gradient, so that the He depletion seen in the atmosphere could be weaker than at Mbar level.

demixing to this equilibrium abundance x_A . If the convective overturn timescale is much shorter than the timescale of thermal cooling of the entire planet, a steady state can be reached where the entire region above the He-rain region will attain the equilibrium abundance x_A . In the adiabatic, convective case, we therefore expect to see this equilibrium abundance in the atmosphere and set $Y_{\text{atm}} = Y_A$. This procedure is the same as in (Nettelmann et al, 2015).

2.4.2 Atmospheric He abundance with TBL

Adiabatic, convective models fail to explain the observed luminosities of Uranus and Neptune (Scheibe et al, 2019). Deviations from the adiabatic, convective baseline case $Y_{\text{atm}} = Y_A$ are therefore expected.

In another series of models we assume that a thermal boundary layer (TBL) exists between the Z -poor outer region and the Z -rich inner region (see Figure 3, right panel). In Uranus and Neptune, this transition occurs in the ~ 10 GPa region (see Sec. 2.2). The idea is that if both envelopes were connected by convective motions, they would have erased the Z -gradient over time (see Figure 3, left panel). A Z -gradient itself inhibits convection unless it is accompanied by a sufficiently strong, de-stabilizing temperature gradient. However, the initial heat budget deep in Uranus, and presumably also Neptune, does not seem high enough to wipe out its entire Z -gradient (Vazan and Helled, 2020). If the Z -gradient inhibits convection, it also reduces the transport of heat. This is a TBL.

A TBL influences the thermal evolution. Conversely, as the outer convective region cools efficiently while the region interior to the stabilizing Z -gradient cannot, a super-adiabatic temperature gradient builds up over time across the TBL. Once the temperature gradient is strong enough, either convective mixing sets in (Vazan et al, 2015) or heat diffusion becomes efficient enough to release heat from the deep interior. In the latter case it has been shown that Uranus and Neptune could appear initially fainter than a planet without a TBL, while after some time they could appear brighter (Scheibe et al, 2021). Thermal evolution models easily place Neptune on the bright side today, whereas due to the stronger incident flux received by Uranus, thermal evolution models that produce effective temperatures close to the observed one of 59 ± 1 K suggest that its outer envelope entered a state of thermal equilibrium with the incident flux quite some time ago, which dramatically slows down the cooling of the deep interior (Scheibe et al, 2021). Models that assume that the barrier to convection existed since early on predict that most of the primordial heat is still conserved today. Such models thus have a strong temperature increment of up to ~ 8000 K across the TBL, which is stabilized by a strong compositional gradient, except perhaps toward the very top of the TBL where the temperature is low and the luminosity high (Scheibe et al, 2021). One could also imagine that the Z -gradient formed later in the evolution, perhaps as a result of $\text{H}_2/\text{H}_2\text{O}$ phase separation (Bailey and Stevenson, 2021). In that case, the present temperature increment could amount to only a few 100 to few 1000 K (Scheibe et al, 2021).

From a structure models perspective, Neuenschwander et al (2024) quantify the temperature increment by comparing their piecewise polytropic profiles to equations of state. If the condition of constant entropy at homogeneous composition is violated, they determine the minimum increment in Z and the depending maximum increment in T that would keep the layer locally Ledoux-stable. Unsurprisingly they arrive at rather large temperature increments with a minimum and mean of respectively $\Delta T = 3000$ K and 8000 K in the 0.6–0.8 R_U region where this effect is most pronounced.

In this work we represent a TBL by a sharp temperature jump at 10 GPa. While guided by interior models that fit the gravity data, this choice matters. The deeper the assumed TBL is located, the less sensitive to thermal effects will be the EOS and the adiabat. Stronger temperature increments could therefore be possible for deeper assumed TBLs. However, we expect a variation within the 10 to 20 GPa range to have a minor effect, and therefore, the fixed mass-shell location at $13 M_E$ as assumed in Scheibe et al (2021), which for present Uranus is at ~ 20 GPa, not to be responsible for the much larger ΔT values found to be necessary to explain the luminosity in some of their evolution models than if they had chosen 10 GPa.

We vary ΔT between 0 and the maximum where the deep interior becomes too warm for H/He demixing to occur. The effect of the TBL on Y_{atm} is only through the warmer deep interior. We do not model the reduced particle transport across the TBL. While this is an obvious inconsistency, it allows us to estimate the minimum Y_{atm} as a function of ΔT given its location.

3 Observed Atmospheric Helium Abundances

For all four outer planets there are data from the combined analysis of Voyager occultation and IR remote sensing (Gautier et al, 1981; Conrath et al, 1984, 1987, 1991) as well as values from various independent sources. What has been declared the *final* Voyager values is shown by grey symbols in Figures 4–6; revised and other observed He abundances are shown as black symbols.

Jupiter: observations

The Galileo entry probe value of $Y=0.238 \pm 0.005$ (von Zahn et al, 1998) suggests that some He rain did occur. As both the mass spectrometer and the He abundance detector (HAD) aboard the Galileo entry probe yielded consistent results (Niemann et al, 1998; von Zahn et al, 1998), these entry-probe measurements are generally considered reliable. In Figures 4–6 we plot the Galileo/HAD measurement of Y_{atm} and $T_{1\text{bar}}$ ($166.1 \pm 0.8\text{K}$) as a dark-red dot. As the in-situ measurements were made in a hot spot, this temperature however may not be representative of Jupiter’s global $T_{1\text{bar}}$; moreover, Voyager I observations indicated a latitudinal variation in $T_{1\text{bar}}$ by $\sim 7\text{K}$ across the equator. The Voyager data have been reanalyzed recently (Gupta et al, 2022), which results in a current $T_{1\text{bar}}$ estimate of 164–174 K; this is +4 K higher than the original Voyager estimate (Lindal, 1992). A re-analysis was kind of overdue as temperatures inferred from radio occultations depend on the composition of the atmosphere, and the helium abundance used for the Voyager occultation analysis was lower than the later Galileo value.

Saturn: observations

Despite several efforts to determine Saturn’s atmospheric He abundance, we cannot tell which one, if any, of the measured values reflect Saturn’s true He abundance. The measurements include a mole fraction of $q_{\text{H}_2} = 0.90 \pm 0.03$ from Pioneer II occultation and IR remote sensing (Orton and Ingersoll, 1980), $Y_{\text{atm}} = 0.18\text{--}0.25$ from Voyager IRIS only (Conrath and Gautier, 2000), $Y_{\text{atm}} = 0.158\text{--}0.217$ from stellar occultations and Cassini UV remote sensing (Koskinen and Guerlet, 2018), $\text{He}/\text{H}_2 = 0.10\text{--}0.16$ from the INMS mass spectrometer at Cassini Grand Finale Tour (Waite et al, 2018), and $Y_{\text{atm}} = 0.075\text{--}0.130$ from Cassini CIRS (Achterberg and Flasar, 2020).

Where the ratio $q_{\text{He}}/q_{\text{H}_2}$, short He/H_2 , is provided, we convert it to Y_{atm} using

$$Y_{\text{atm}} = \frac{m_{\text{He}} \text{He}/\text{H}_2}{m_{\text{He}} \text{He}/\text{H}_2 + m_{\text{H}_2}} \quad (1)$$

with $m_{\text{He}} = 4.0026$ and $m_{\text{H}_2} = 2.0158$ (Conrath et al, 1987). Where the mole fraction q_{He} is provided without clear indication of the mole fractions of other species like methane or N_2 , we convert according to

$$Y_{\text{atm}} = \frac{m_{\text{He}} q_{\text{He}}}{m_{\text{He}} q_{\text{He}} + m_{\text{H}_2} (1 - q_{\text{He}})} \quad (2)$$

with $q_{\text{He}} + q_{\text{H}_2} = 1$.

Uranus and Neptune: observations

Early analysis of the Voyager data suggested that the atmospheres of Uranus (Conrath et al, 1987) and Neptune (Conrath et al, 1991) have preserved the protosolar value, with perhaps a slight enhancement in Neptune (Atreya et al, 2020). However, the He abundance from occultation data is inferred from the mean molecular weight, and thus different abundances of methane or other atmospheric constituents would result in a different inferred helium abundance. Sromovsky et al (2011) found that IR spectra taken by Voyager 2 and near-IR spectra taken by HST are better explained by a 2.3–4% methane volume mixing ratio above a thick methane cloud deck compared to its neglect in the *final* analysis of the occultation data by (Conrath et al, 1987). According to Sromovsky et al (2011) the Voyager refractivity profiles would therefore be better explained by a lower He abundance implying a moderate depletion for Uranus. We convert the He/H₂ mixing ratios of their models D1, F1, D, to He mass abundance using Eq.1.

A similar effect is seen for Neptune, where inclusion of 0.3% N₂ shifts the He abundance downward to around the protosolar level (Atreya et al, 2020).

4 Results for the Atmospheric Helium Abundance

The 1-bar temperature serves the interior models as an outer boundary condition for the adiabat. The higher $T_{1\text{bar}}$, the warmer the adiabatic interior. For high enough $T_{1\text{bar}}$ a protosolar abundance of helium will remain fully miscible in the hydrogen-environment. This means that we expect the atmosphere of a warm planet to be of protosolar H/He ratio, $Y_{\text{atm}} = Y_{\text{proto}}$ unless other processes than H/He immiscibility act to modify the atmospheric H/He ratio. The lower $T_{1\text{bar}}$, the colder the adiabat. With decreasing $T_{1\text{bar}}$, a planetary adiabat will eventually begin to overlap with the H/He demixing diagram. The colder the adiabat, the lower is the equilibrium abundance Y_A . According to this simple model, we expect to see a stronger atmospheric helium depletion with respect to the protosolar value the lower the $T_{1\text{bar}}$ of the planet.

In Figures 4–6 we compare our predictions of the atmospheric helium depletion due to H/He phase separation at depth to the observed atmospheric He abundances of the outer planets.

Overall we note a strong influence of the phase diagram and of the H/He EOS used. CD21-EOS yields the coldest adiabats and therefore the strongest depletion. CMS-19 EOS yields the highest temperatures at 1 Mbar, but not at 2 Mbars, where H/He-REOS is warmer. To reach the equilibrium concentration at the tangential P_{touch} , which is typically somewhere in between, apparently a less strong depletion is needed than for REOS. This is an effect of the slopes of the adiabat and the demixing curves.

Since the SR18 phase diagram has the lowest demixing temperature at protosolar He abundance, the initial entry into the demixing regions occurs at the lowest 1-bar temperatures. But since the temperature are rather low upon first entry and the isobaric demixing temperatures are rather flat with decreasing He abundance (Fig. 1), the equilibrium He abundance must fall steeply with decreasing $T_{1\text{bar}}$. The opposite holds for the BLM21-data, where the entry-point occurs at high $T_{1\text{bar}}$. As a result, Y_{atm} falls slowly with $T_{1\text{bar}}$ for BLM21-N23.

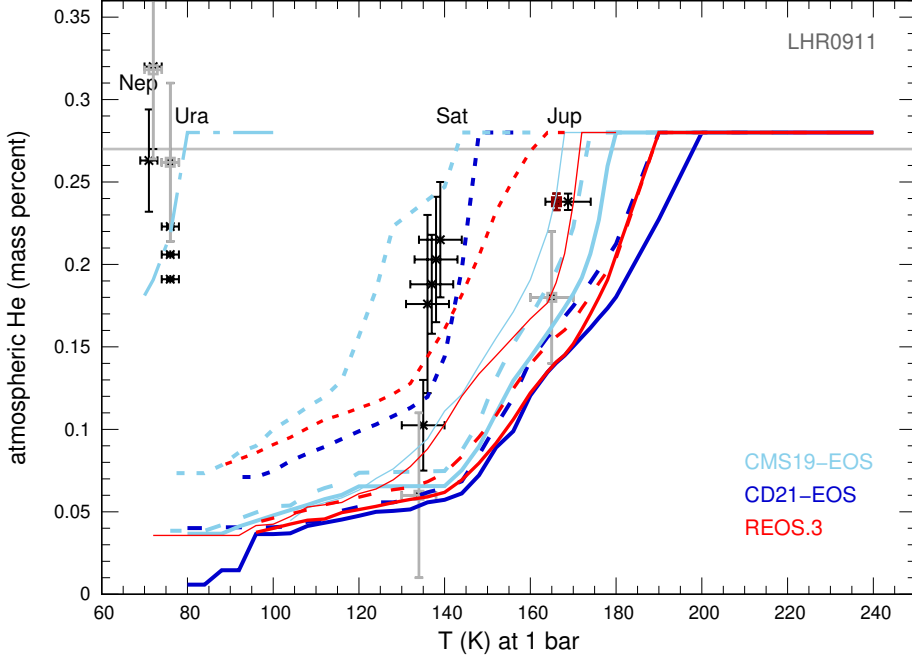


Fig. 4 Atmospheric He abundances in the giant planets from observations (grey, black symbols with error bars) and predicted (lines) by the BLM21-N23 H/He phase diagram and the three different H/He-EOS REOS (red), CD21 (blue), CMS19 (light blue). Symbols: grey symbols are the *final* Voyager data for Jupiter and Saturn (Conrath et al, 1984), Uranus (Conrath et al, 1987), and Neptune (Conrath et al, 1991) displayed at the Voyager 1-bar temperatures of Lindal (1992). Black dots for Saturn and Neptune are slightly shifted in $T_{1\text{bar}}$ for readability. Black symbol for Neptune: revised Voyager with 0.3% N_2 (Atreya et al, 2020); black symbols for Uranus: models D1, F1, G with enhanced methane abundances (Sromovsky et al, 2011); Lines: Thick lines are for the $Z_{H_2O} = 0$ (solid), 0.5 (long dashed) and 0.9 (dotted). Thin solid lines are for constant shifts in T_{dmx} chosen to reproduce the Galileo entry probe value of Jupiter, here $dT_{\text{dmx}} = -400(420)$ K for CMS19(REOS). Dashed-dotted lines are for ice giant models with a thin thermal boundary layer at 10 GPa across which the temperature increases, here by $\Delta T = 2000$ K (CMS19), and $Z = 0$. Grey horizontal line indicates protosolar value of $Y_{\text{proto}} = 0.27$.

The He/H dilution-effect with increasing Z can clearly be seen in form of a reduced He depletion, but this effect becomes relevant only for $Z > 0.5$. For $Z = 0.9$, the REOS-adiabats show stronger depletion than the CD21-adiabats. This is the effect of the temperature-influence of Z on the ideal-entropy of mixing to make the adiabat colder, and since this effect is included only for REOS-adiabats, the REOS-adiabat becomes colder while the CD21 adiabat does not at high- Z . Colder adiabats lead to stronger depletion.

Jupiter: predictions

Given the uncertainties in the H/He phase diagram, in the H/He EOS, in Jupiter's internal structure, and our simplifying assumption of an adiabatic interior, it is not to be expected that the Galileo value would right-away be reproduced by our atmospheric helium depletion model.

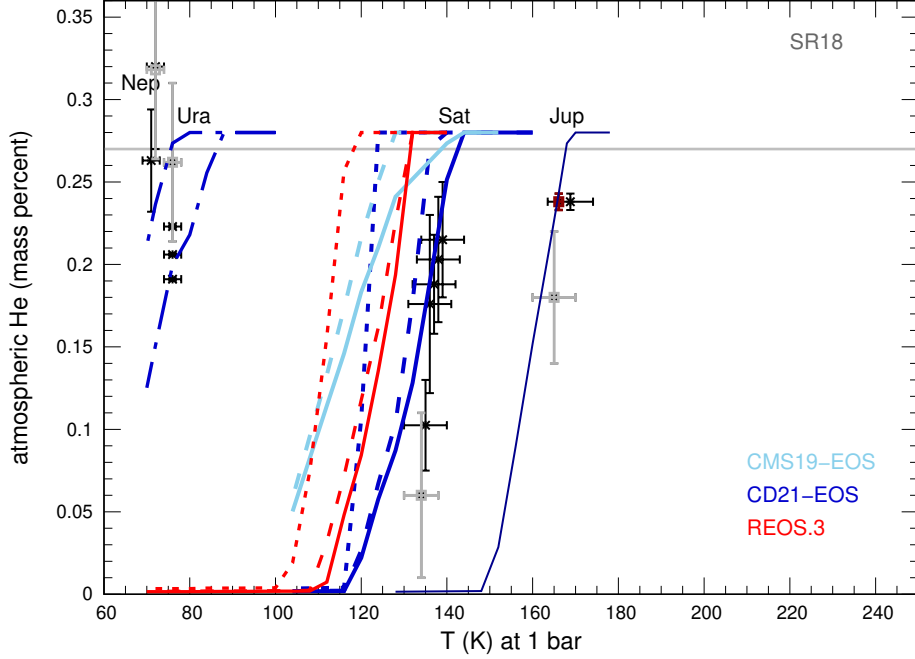


Fig. 5 Same as Fig. 4 but for the SR18 H/He phase diagram and a TBL with $\Delta T=1300$ or 1500 K (CD21) and a phase diagram shift of $+1000$ K (CD21).

For the SR18 phase diagram (Fig. 5), Jupiter seems to be too warm for demixing to occur regardless of the EOS. On the contrary for to BLM21-N23 (Fig. 6) Jupiter would experience very strong depletion of $Y \sim 0.1$ almost regardless of the H/He EOS and $Z < 0.5$. With LHR0911, the depletion is around 0.15.

Let us assume that some of the uncertainties in regard of the phase diagram and the EOS can be captured by shifting the phase diagram in temperature to match the Galileo value. That procedure has been adopted before (Nettelmann et al, 2015; Mankovich and Fortney, 2020) to compute the influence of helium rain on the evolution of Jupiter. In a pioneering study, Fortney and Hubbard (2003) shifted the phase diagrams of that time to reproduce the luminosity of Saturn. For the LHR0911 H/He phase diagram only a moderate shift by ~ 400 K is needed which is well within the uncertainty of ± 500 K of the phase diagram. Shifting the phase diagram vertically in temperature leads to a horizontal shift in the $Y_{\text{atm}}(T_{1\text{ bar}})$ curves. Any combination that reproduces the Galileo value predicts a rather strong He depletion for Saturn of 0–0.14.

Saturn: predictions

The top of the demixing region in Saturn begins between $0.65 R_{\text{Sat}}$ (1 Mbar, LHR0911) and $0.55 R_{\text{Sat}}$ (2 Mbar, SR18), which is deeper inside than in Jupiter where the 1 Mbar region is at $0.86 R_{\text{Jup}}$ and 2 the Mbar level at $0.81 R_{\text{Jup}}$.

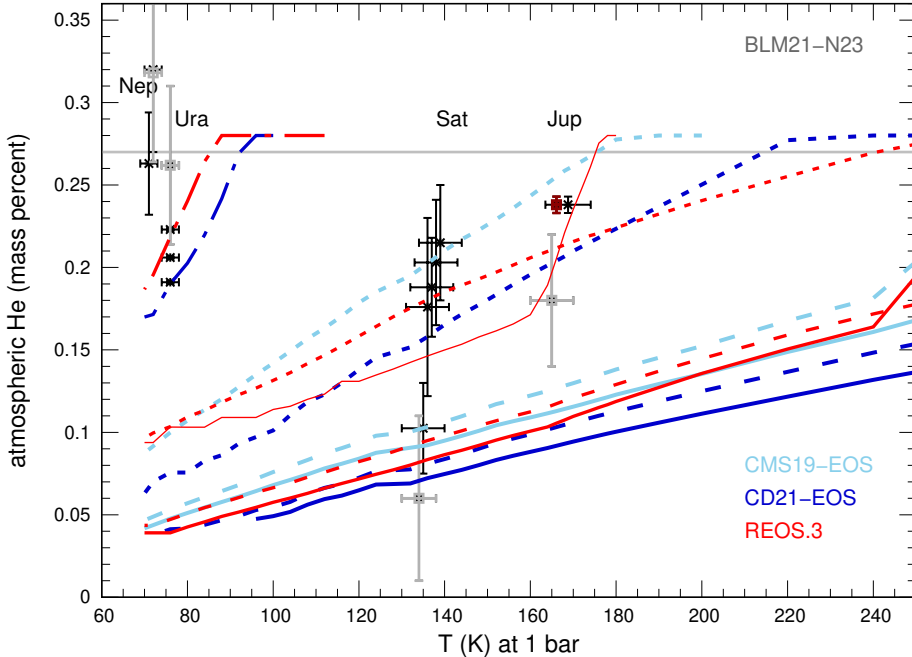


Fig. 6 Same as Fig. 4 but for the BLM21-N23 H/He phase diagram and a TBL with $\Delta T = 3500$ K (CD21, REOS.3) and a phase diagram shift of -2820 K (REOS.3).

One may think that knowledge of Saturn’s tropospheric He abundance in addition to that of Jupiter could help constrain the H/He phase diagram: a prediction that works for Jupiter should also work for Saturn if Saturn’s outer envelope is similar to that of Jupiter. Adjusted to Jupiter (thin solid lines) or not, both LHR0911 and the BLM21-N23 data predict $Y_{\text{atm}} < 0.14$ for Saturn. In contrast, the SR18 diagram with the CD21-EOS predicts moderate depletion of 0.15–0.25 for Saturn.

In Section 5.2 we discuss the inversion of what a measured value for Saturn by an entry probe could imply for the interior structure and the phase diagram. However we caution that further planet properties may influence the atmospheric helium abundance rendering the inversion to be non-unique. An important such property would be an outer stable layer above the He-rain zone (OSL). Such has been suggested for Jupiter as a reason for the slow-down of the zonal winds and to be necessary to maintain zonal winds at high latitudes within the tangent cylinder (Wulff et al, 2022). A stable layer can be sub-adiabatic or super-adiabatic. A sub-adiabatic OSL (sub-OSL) could be caused by a radiative zone due to alkali metal depletion (Guillot et al, 1994), which indeed may be needed to explain Jupiter’s low opacity in the ~ 1 kbar region as observed by Juno (Bhattacharya et al, 2023). A subOSL would lead to colder interiors and thus stronger He-rain. In this case the He depletion in the atmosphere would be weaker than in the Mbar region: a de-stabilizing inverted Y -gradient. A super-adiabatic OSL (supOSL) is a TBL. It implies warmer interiors with weaker He

depletion at depth. The He-abundance in the atmosphere can be higher than depth: a de-stabilizing inverted Y-gradient and be higher than in the adiabatic case.

To stabilize a super-adiabatic layer against convection an additional Z-gradient is required. This is consistent with current Saturn and ice giant structure and models but not with current Jupiter models. Thus a supOSL is an option for Saturn but not for Jupiter. An OSL offers options to bring both Jupiter and Saturn under one umbrella even with the cold SR18 phase diagram and the cold CD21 adiabat, which otherwise seems difficult according to Figure 5.

Uranus and Neptune: predictions

Under the assumption of an adiabatic interior, the LHR0911 H/He phase diagram predicts a strong ($Y_{\text{atm}} < 0.1$) He depletion in the cold atmospheres of Uranus and Neptune. If there is a TBL, the deep interior will be warmer, and helium depletion at depth will be seen with a delay in the atmosphere due to the finite diffusivities of He atoms. By neglecting this delay we overestimate the He depletion. The respective dot-dashed curves in Figs. 4–6 are thus lower limits to Y_{atm} . For $\Delta T > 4000$ K the interior would become so warm that H/He-phase separation can not occur in any of the considered cases.

With the help of a TBL, moderate depletion can be obtained, in agreement with the revised Voyager measurements of Uranus. However, the depletion is highly sensitive to ΔT . As argued above, ΔT could be smaller with a stronger He depletion at depth but a delayed observable depletion in the atmosphere, but ΔT could also be larger for a deeper TBL.

Some of the evolution models that are adjusted to reproduce the luminosity of Uranus and Neptune (Scheibe et al, 2021) and some structure models (Neuenschwander et al, 2024), suggest that ΔT could also be substantially larger in which case no depletion at depth occurs and thus no depletion in the atmosphere.

This leaves us with (at least) two options for Neptune: (i) Helium is present at depth but due to a strong TBL, H/He phase separation does not occur; (ii) Helium is not present at depth.

5 Discussion

5.1 H/He phase diagram.

It has become common to shift the phase diagram in temperature to reproduce the Galileo value under the assumption of an adiabatic interior (Fortney and Hubbard, 2003; Nettelmann et al, 2015; Mankovich and Fortney, 2020). That a modification of the LHR0911 data set is needed to match the Galileo value is not surprising, as that data set neglects non-ideal contributions to the entropy of mixing and therefore can come close to the real demixing behavior, which we stress is still unknown, only by coincidence. That the required shift in temperature of ~ 400 K (with CMS19 and REOS) is well within the uncertainty of ± 500 K at 1 Mbar to ± 1000 K at Mbar (Lorenzen et al, 2009) of the data set itself suggests that such a coincidence could indeed be the case.

On the other hand, the Galileo probe value may not be right-away reproduced for other reasons. For instance, Jupiter’s interior may not be fully adiabatic. A stably stratified layer atop the demixing region is required by magnetic field models (Moore et al, 2022) and in order to slow-down the zonal flows (Christensen et al, 2020; Wulff et al, 2022).

Consider a H/He phase diagram that reproduces the Galileo value for an assumed adiabatic interior while the real interior has a stable layer above the demixing region. If super-adiabatic, the stable layer would then require an upward shift $\Delta T_{\text{dmx}} > 0$ of this phase diagram. If sub-adiabatic, the stable layer may require a downward shift $\Delta T_{\text{dmx}} < 0$ or an upward shift. If the applied H/H phase diagram seems to over-estimate the atmospheric He abundances in Jupiter, like the SR18 one does, introduction of a subadiabatic OSL is the only way to reduce the atmospheric value. If the applied H/He phase diagram seems to under-estimate Jupiter’s atmospheric value, both a subOSL or a supOSL can lift Y_{atm} upward. Quantitative assessments are needed. Knowledge of the H/He phase diagram therefore provide valuable information on Jupiter’s interior structure. More experimental efforts are needed to constrain the H/He phase diagram.

5.2 Gas Giant Internal Structure

Let us assume the H/He phase diagram is uncertain within the range given by SR18 on the cold end and BLM21-N23 on the warm end, and that the adiabatic P - T profile is uncertain within CD21 on the cold end and CMS19 on the warm end around 1 Mbar and REOS at higher pressures. We here consider several inverted cases to see what, if anything, a potential Saturn entry probe He abundance measurement could teach us about the H/He phase diagram or the internal structures of Jupiter and Saturn. We consider the two extreme cases. Case (1) is a warm BLM21-N23 like phase diagram and cold CD21-like adiabat, which leads to strong He depletion inside Jupiter. Case (2) is a cold SR18-like phase diagram and a warm adiabat, which leads to no demixing in Jupiter. Suppose a Saturn entry probe measures:

- *He/H in Saturn equal to Jupiter in case (1)* Jupiter in this case must¹ have a SSL atop the demixing region. Also Saturn must have a SSL and it must be less permissible than in Jupiter. What is seen in the atmosphere reflects the properties of the SSL. These properties must be able to explain the subsolar Ne/He in Jupiter’s atmosphere. Knowing Ne/He for Saturn would place additional constraints on the SSL.
- *He/H in Saturn much less than in Jupiter in case (1)* Jupiter must have a SSL. Saturn may have a Jupiter-like SSL. The lower He/H in Saturn’s atmosphere occurs because He-rain in Saturn begun earlier in the evolution so He atoms had more time to travel through the SSL.
- *He/H in Saturn higher than in Jupiter in case (1)* Jupiter must have a SSL. Saturn must have a thick SSL. While a thick SSL is indicated by the seismic data, that SSL would occur deeper inside underneath the He-rain region (Mankovich and Fuller, 2021). If sub-adiabatic, it acts to shield the atmosphere from the He-depletion at

¹The word ‘must’ abbreviates ‘may have, among alternative explanations which escaped our perception’

depth. If super-adiabatic it acts to keep the interior so warm that He-rain does not or if so occurs only weakly in Saturn. Indeed, [Leconte and Chabrier \(2013\)](#) have suggested that a permanent thick SSL with a Z-gradient could have prevented Saturn’s deep interior from efficient cooling so that today, Saturn’s excess luminosity would result from primordial heat floating along a superadiabatic gradient rather than from the gravitational energy released by falling He droplets. This is a cold Jupiter and warm Saturn case.

- *He/H in Saturn much less than in Jupiter in case (2)* Jupiter must have a subSSL because of the phase diagram. The sub-adiabaticity in this case is mandatory in order to have a cold enough deep adiabat for He-rain to occur. An SSL is not needed for Saturn.
- *He/H in Saturn higher than in Jupiter in case (2)* Jupiter must have a subSSL because of the H/He phase diagram, Saturn as well.

None of the considered cases excludes a particular phase diagram.

5.3 Ice Giant Internal Structure

Let us assume we knew the H/He phase diagram and the H/He-EOS precisely. This leaves us with several options of what to expect for the atmospheric helium abundance of the ice giants depending on their internal structure. We list some cases below from the point of view of a putative probe-measurement.

- *Protosolar H/He.* If there is no helium deep inside, H/He phase separation does not take place, and therefore we would expect to see the protosolar value in the atmosphere unless there are other chemical processes that affect hydrogen and helium differently. Observations indicate a protosolar H/He ratio in the atmosphere of Neptune ([Atreya et al, 2020](#)). The currently rather large uncertainty in the low-order gravitational harmonics of Neptune permits a rather wide range of internal compositions. One of such compositions is a pure water, H/He-free deep interior if the entire planet is assumed to be adiabatic ([Nettelmann et al, 2013](#)), or with some admixture of rocks if it is warmer ([Nettelmann et al, 2016](#)). Thus a He-free deep interior is an option for Neptune.

We can also expect to see the protosolar ratio if there is helium deep inside and H/He phase separation does take place, but if the particle exchange between the interior and the atmosphere is strongly inhibited. An indication for a barrier to particle transport could be that the deep interior below a few GPa or a few tens of GPa is more enriched in heavy elements than the outer region ([Nettelmann et al, 2013](#)) for a wide range of thermal profiles ([Podolak et al, 2019](#)). A barrier to convection in regard of inhibited heat transport is a possible solution to explain the low luminosity of Uranus ([Nettelmann et al, 2016](#); [Scheibe et al, 2021](#)) and the high luminosity of Neptune ([Scheibe et al, 2021](#)).

In addition, we would expect no atmospheric He depletion if the deep interior were much warmer than along an adiabat. Strong temperature increments > 3000 K can explain the luminosity of both planets ([Scheibe et al, 2021](#)) and are predicted by some polytropic structure models ([Neuenschwander et al, 2024](#)).

In all of these cases one would expect a protosolar or slightly enhanced Ne/H ratio, as Ne will not be removed from the atmosphere by partitioning into falling He droplets at depths (Stevenson, 1998) but may be slightly enriched if the accreted nebular gas was H/He-depleted.

- *Strong Atmospheric Helium depletion.* Strong atmospheric helium depletion in Uranus and Neptune is predicted by any of the considered H/He phase diagrams and their modifications, simply because their surface temperatures of ~ 75 K are so much lower than those of Saturn (~ 135 K) and Jupiter (~ 170 K); if the gas giants experience H/He phase separation, so would planets with colder adiabats even more. This scenario implies that the interiors of Uranus and Neptune are adiabatic and do exchange particles with the atmosphere, and that helium is present at depths of Mbars. We showed that even for high ice mass fractions of up to 90%, consistent with structure models, He-rain would strongly deplete the region above to levels of $Y_{\text{atm}} \ll 0.1$

In this case one would also expect to see a strong Ne/H depletion, as Ne will be removed by partitioning into falling He droplets.

- *Weak Atmospheric Helium depletion.* On Uranus, a weak atmospheric helium depletion is indicated by the observed mean molecular weight profile inferred from the Voyager occultation experiment if an enhanced methane abundance is assumed as would best explain the IR and near-IR spectra (Sromovsky et al, 2011). Our model of H/He phase separation predicts weak helium depletion if the (shifted) LHR0911 data are used and most importantly, if a super-adiabatic thermal boundary layer is assumed that inhibits but not totally suppresses the particle and heat exchange. We find that the increment in temperature across the TBL must not exceed 1300–4000 K at a pressure level of 10 GPa in order to keep the deep adiabat cold enough. The change in temperature could perhaps be as small as a few 100 K if the TBL delayed the particle transport and thus the depletion of the atmosphere. Without that effect values of 1300–4000 K are favored depending on the H/He phase diagram, EOS, and deep water abundance. A TBL of the order of a few 100 to a few 1000 K is consistent with the high luminosity of Neptune if it established a few 100 Myr after its formation (Scheibe et al, 2021). In this case Ne/H could be depleted as well, depending on the onset of He-rain and the timescale of neon diffusion compared to helium diffusion through the TBL.

Even though the 1-bar temperatures of Uranus (72 ± 2 K) and Neptune (76 ± 2 K) are very similar as compared to those of Saturn (135 K) and Jupiter (170 K), our models with a TBL that yield weak He depletion for Uranus predict a stronger depletion for Neptune due to this small 4 K difference. This is in contrast to observations, which show a higher He abundance in the atmosphere of Neptune (Atreya et al, 2020). The different atmospheric He abundances may be a sign of different internal structures (Helled and Fortney, 2020).

- *Atmospheric He enrichment.* An atmospheric enrichment in helium might be possible if phase separation processes take place that affect hydrogen and helium differently. Phase separation of water from hydrogen has been suggested to explain the reduced heavy element abundances in the outer envelopes of Uranus and Neptunes as revealed by their observed gravity data (Bailey and Stevenson, 2021).

Rain-out of water would reduce the amount of water in the deep atmosphere down to a level which is dictated by the $\text{H}_2/\text{H}_2\text{O}$ phase diagram but leave the atmospheric He/H ratio unaffected. Simultaneously, H_2 would rise from the deep interior upward until the concentration of the remaining H_2 is low enough to be miscible in the ionic water environment (Bailey and Stevenson, 2021). Limited solubility of H_2 gas in salty water is also seen in laboratory experiments that were conducted to investigate the storage of gaseous H_2 in underground water reservoirs (Salaheddine et al, 2020), which happens to be at P - T conditions of ~ 200 bars and ~ 350 K along the Neptune adiabat. Rising H_2 would enrich the atmosphere and let it appear depleted in helium. However, the miscibility of helium in ionic water is not so well studied, and helium may rise as well.

An enrichment in He could also be seen if large amounts of CO or other carbon-bearing species were absorbed by the planet. These could then react with H_2 in the hydrogen-environment to form methane and water. Whether the amount of H_2 particles that can be bound in form of volatiles is sufficient to deplete the atmosphere in H_2 and let it appear He-enriched remains to be estimated.

An enrichment in He could also be possible if He atoms prefer to partition into the molecular-hydrogen layer before forming droplets that would rain-out because of their higher mean molecular weight (Stevenson and Salpeter, 1977b,a). To address the behavior of He once the Gibbs free energy difference suggests phase separation may be studied in direct computer simulations with He atoms in molecular and metallic hydrogen, respectively.

One may think that a He enrichment could occur due to late formation in an evaporating protosolar disk, as the lightest elements may escape first and thus leave behind a gas component that is primarily depleted in hydrogen. In that scenario however, the apparent enrichment in the noble gases should increase with their molecular weight. Guillot and Hueso (2006) showed that the escape of disk gas would occur hydrodynamically without separation of the species in the disk gas. The reason why the remaining disk would be equally enriched in the heavy noble gases Ar, Kr, Xe, and perhaps explain their enrichment in the atmosphere of Jupiter, is that these elements can be captured by grains that settle onto the disk midplane, where the planets form.

5.4 Gravity

The uncertainty in interior structure and composition is partially due to the magnitude in the uncertainty of the observational constraints and their limited number. For instance, current interior models of the outer planets are constrained by the low-order gravitational harmonics J_2 and J_4 . The uncertainty in the J_4 values of Uranus and especially of Neptune allows for a wide of interior models (Kaspi et al, 2013; Nettelmann et al, 2013; Movshovitz and Fortney, 2022). Knowing the depth of the zonal winds would constrain the dynamic correction to J_4 and thus could eliminate a large fraction of the models (Kaspi et al, 2013). Deep winds at depths of the order of 1000 km also change the higher order moments J_6 and J_8 by a significant amount of 20% and 30%, respectively (Neuenschwander and Helled, 2022). Movshovitz and Fortney

(2022) also showed that J_6 and J_8 constrain the range of deep interior density distribution much tighter for the ice giants than they do for Jupiter and Saturn. It is to be expected that a measurement of the higher-order moments J_6 and J_8 for Uranus and Neptune would reduce the current variety of possible models, both directly and through inference of the wind depth. Such measurement can only be achieved by an Orbiter mission.

6 Summary

We have applied three H/He phase diagrams (LHR0911,SR18,BLM21-N23) and three H/He-EOS (CMS19,CD21,REOS.3) and assumed a wide range of deep water abundances (0–0.9) as well as the presence of a thermal boundary layer (TBL) for the ice giants to address He depletion in the outer giant planets. Our conclusions are as follows.

1. We expect to see strong depletion in He in the atmospheres of both Uranus and Neptune if their deep interiors are adiabatic and contain H/He.
2. The observed weak helium depletion in the atmosphere of Uranus might be indicative of a moderate TBL and the presence of H/He in its deep interior.
3. The observed protosolar He/H ratio in the atmosphere of Neptune might be indicative of a helium-free deep interior composed of ices and rocks.
4. If the interiors of Uranus and Neptune are similar, our models predict a slightly stronger helium depletion for Neptune than for Uranus, contrary to what is observed. This suggests their interiors are dissimilar to some extent.
5. Considering atmospheric enrichment in helium is beyond the scope of this work but could happen in the Ice Giants as a result of hydrogenization of abundant CO.
6. For Saturn, we expect any He depletion as a result of uncertainties in the interior structure, although most attempts to reconcile a potentially measured value with the jovian value given a H/He phase diagram requires the presence of an outer stable layer (OSL) in both planets.
7. For Jupiter, all considered H/He phase diagrams may explain its observed H/He depletion but all require the presence of an outer OSL. Cold demixing curves (SR18) require a sub-adiabatic OSL.
8. Explaining both Jupiter and Saturn with the same H/He phase diagram seems problematic if their interiors are adiabatic. Conversely, this issue is immediately lifted if an OSL is allowed for.
9. More experimental constraints on the H/He phase diagram are urgently needed given the powerful implications of the phase diagram on the interior structure of the giant planets, especially in conjunction with a measured atmospheric He abundance.
10. While here we focused on helium only, an in-situ measurement of the abundances of Ne and heavier noble gases in addition to that of He would tremendously help to inform us about the deep composition and the atmosphere-interior coupling in the giant planets.

The science addressed in this work requires improved knowledge of the H/He phase diagram and an entry probe down to the levels of ~ 5 bars that is equipped with a

mass spectrometer to one of the ice giants but best also to Saturn. The science return from an entry probe does not depend critically on a launch window. Hence an Uranus Entry Probe-centered mission design such as the UOP (Mandt, 2023) may compete against lighter mission designs that trade the science objectives for lower cost and earlier launch time (Cohen et al, 2022).

Acknowledgments. N.N. acknowledges support through NASA’s Juno Participating Scientist Program under grant 80NSSC19K1286. This work was also supported by the DFG Research Unit FOR2440/2 under grant NE1734/2-2. We thank Armin Bergermann for providing the tabulated data of the SR18 phase diagram and the two referees for constructive comments that helped us to improve the paper.

Declarations

- Funding: Partial financial support was received from NASA under Grant 80NSSC19K1286 and from the German Science Foundation (DFG) under Grant NE1734/2-2.
- Conflict of interest: The authors have no competing interests to declare that are relevant to the content of this article.

Appendix A Construction of the BLM21-N23 phase diagram

This Section reports our construction of a H/He phase diagram that is based on the experimental data of Brygoo et al (2021). We label it BLM21-N23 and have constructed it as simple as described below.

Brygoo et al (2021) provide a demixing curve for 11% He mol fraction. The curve interpolates between four important experimental data points in P - T space. At the point at $P = 0.93$ Mbar and $T = 4700 \pm 200$ K the reflectivity is found to increase with increasing pressure to levels that are found to be characteristic of a H-rich/He-poor phase, while at the point at ($P = 1.5$ Mbar, $T = 10.400 \pm 500$ K) the reflectivity decreases. These two points are interpreted to mark, respectively, the entry into and leave from the demixing region. We have estimated the here given uncertainty in T from the figures in (Brygoo et al, 2021). Toward higher pressures, they extend the demixing curve as a flat line up to ~ 2.5 Mbar. Toward lower pressures they draw the demixing curve to run smoothly through two further experimental data points of (Loubeyre et al, 1987) at 6 and 9 GPa, respectively.

First, we construct a demixing line for $x_{\text{He}} = 0.05$ mol fraction between 0.6 and 2 Mbar. Second, we use that curve to construct further demixing curves $T_{\text{dmx}}(x_{\text{He}}; P)$ by linear interpolation in $T(x_{\text{He}})$ at a number of pressure points. Third, we assume a symmetric shape of the phase diagram $T_{\text{dmx}}(x_{\text{He}}; P)$ with respect to the dividing line at $x_{\text{He}} = 0.5$. For all pressures, we set $T_{\text{dmx}}(x_{\text{He}} = 0.5) = T_{\text{dmx}}(x_{\text{He}} = 0.11)$. This ensures a monotonic behavior in $T_{\text{dmx}}(x_{\text{He}})$ in lack of experimental data. For comparison, the increase in the SR18 data along the 2 Mbar isobar over this concentration range is 3300 K while for the LHR0911 data it is 1300 K. However, the $x_{\text{He}} = 0.11$ mole fraction curve corresponds to $Y = 0.33$, which is more He-rich than in Jupiter’s deep

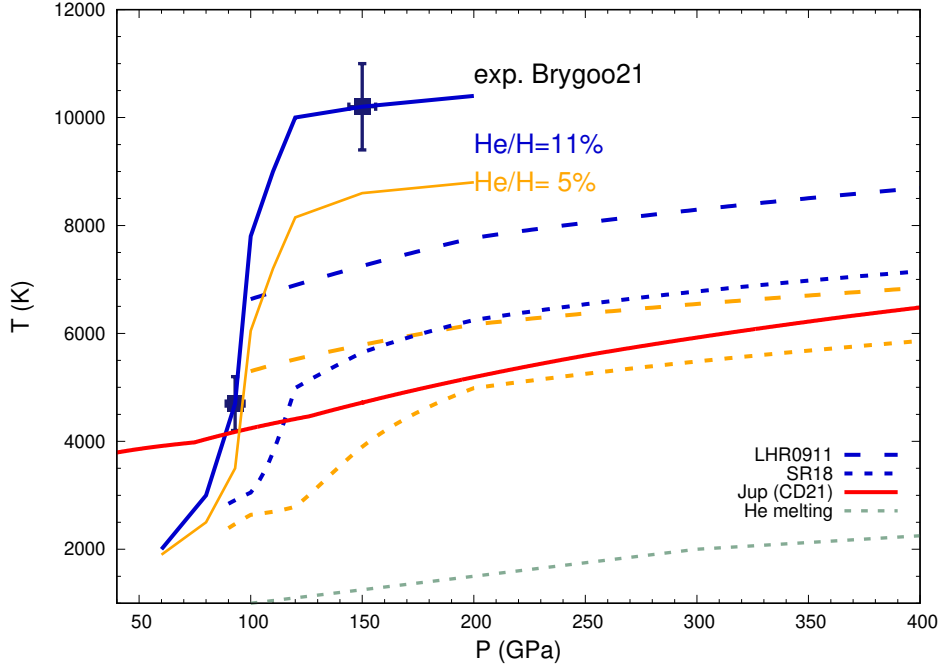


Fig. A1 Constructed H/He-demixing curve at $x_{\text{He}} = 0.05$ (solid orange line) to obtain the BLM21-N23 H/He phase diagram based on the BLM21-demixing line at $x_{\text{He}} = 0.11$ (solid blue line) and the approximate temperature differences at 1.5–2 Mbars in the LHR0911 (dashed) and the SR18 (dotted) data for these two He abundances. The grey-green curve is the He melting line of Ref. (Preising and Redmer, 2019) while the red curve is a Jupiter model based on CD21-EOS (Nettelmann et al in prep).

interior according to models with a He-poor outer envelope of the Galileo entry probe He abundance of $Y = 0.238 \pm 0.005$. Jupiter models do not reach into this high-He abundance region. On the other hand in Saturn’s deep interior the He-abundance can easily reach levels of $Y \sim 0.4$ or higher (Nettelmann et al, 2013; Mankovich and Fortney, 2020) and thus exceed the region of our version of the BLM21 phase diagram where it is supported by data.

To obtain the curve for $x_{\text{He}} = 0.05$ we use the SR18 and LHR0911 data as guidance. At 1.5 Mbars, the temperature difference between $x_{\text{He}} = 0.11$ and 0.05 is -1750K (SR18) and -1500K (LHR0911), while at 2 Mbars the difference is -1260K and -1600K , respectively. We assume an intermediate difference of -1600K at 1.5 Mbar, which because of the flat behavior in the $x_{\text{He}}=0.11$ curve of Brygoo et al (2021) is also assumed for 2 Mbars and beyond. Toward lower pressures we let the temperature difference decrease to -100K at our lowermost pressure of 0.6 Mbar. For comparison, the difference at 0.5 Mbar in the SR18 data is -350K . Our choice of -100K ensures that the $x_{\text{He}} = 0.05$ curve would not intersect with the SR18 curve upon extrapolation but approach it toward lower pressures. At intermediate pressures, we let the temperature decrease by amounts that are chosen to yield a well-behaved curve, which is displayed as the orange line in Figure A1.

On the low- P end, all demixing lines are well above the He melting line (Preising and Redmer, 2019). We also recover the behavior that Jupiter adiabats, if they are cold enough depending on the H/He-EOS used, will intersect with the SR18 protosolar abundance demixing line near 2 Mbars while for the LHR0911 data, at 1 Mbar. Interestingly, the intersection of the displayed Jupiter adiabat, here computed using the CD21-EOS, with the BLM21-N23 diagram can also be expected to occur at ~ 0.9 Mbar. At 0.9–1 Mbars, the demixing temperatures are not that much higher than for the LHR0911 data and therefore, we expect a not that much lower inferred level of He depletion, consistent with our results in Figure 4.

However we caution that our construction of a BLM-N23 H/H phase diagram is not based on the principle of thermodynamic consistency of an underlying H/He EOS but on two reflectivity data points with high experimental uncertainty. More reflectivity measurements and theoretical predictions for H/He mixtures are needed to evaluate such an approach.

References

- Achterberg RK, Flasar FM (2020) Saturn’s Atmospheric Helium Abundance from Cassini Composite Infrared Spectrometer Data. PSJ 1:30. <https://doi.org/10.3847/PSJ/ab9cb6>
- Atreya S, Mahaffy P, Niemann H, et al (2003) Composition and origin of the atmosphere of jupiter—an update, and implications for the extrasolar giant planets. PSS 51:105. [https://doi.org/10.1016/S0032-0633\(02\)00144-7](https://doi.org/10.1016/S0032-0633(02)00144-7)
- Atreya S, Hofstadter M, In J, et al (2020) Deep Atmosphere Composition, Structure, Origin, and Exploration, with Particular Focus on Critical in situ Science at the Icy Giants. SSRv 216:18. <https://doi.org/10.1007/s11214-020-0640-8>
- Bailey E, Stevenson D (2021) Thermodynamically Governed Interior Models of Uranus and Neptune. PSJ 2:64. <https://doi.org/10.3847/PSJ/abd1e0>
- Baraffe I, Chabrier G, Barman T (2008) Structure and evolution of super-Earth to super-Jupiter exoplanets I. Heavy element enrichment in the interior. A&A 482:315–332. <https://doi.org/10.1051/0004-6361:20079321>
- Becker A, Lorenzen W, Fortney J, et al (2014) Ab initio equations of state for hydrogen (H-REOS.3) and helium (He-REOS.3) and their implications for the interior of brown dwarfs. ApJS 215:14. <https://doi.org/10.1088/0067-0049/215/2/21>
- Bethkenhagen M, Meyer E, Hamel S, et al (2017) Planetary Ices and the Linear Mixing Approximation. ApJ 848:67. <https://doi.org/10.3847/1538-4357/aa8b14>
- Bhattacharya A, Li C, Atreya S, et al (2023) Highly depleted alkali metals in jupiter’s deep atmosphere. ApJL 952:L27. <https://doi.org/10.3847/2041-8213/ace115>

- Brygoo S, Loubeyre P, Millot M, et al (2021) Evidence of hydrogen–helium immiscibility at Jupiter-interior conditions. *Nature* 593:517–521. <https://doi.org/10.1038/s41586-021-03516-0>
- Celliers P, Millot M, Brygoo S, et al (2018) Insulator-metal transition in dense uid deuterium. *Science* 361:667
- Chabrier G, Debras F (2021) A New Equation of State for Dense Hydrogen-Helium Mixtures. II. Taking into Account Hydrogen–Helium Interactions. *ApJ* 917:4
- Chabrier G, Mazevet S, Soubiran F (2019) A New Equation of State for Dense Hydrogen-Helium Mixtures. *ApJ* 872:51
- Chang X, Chen B, Zeng Qe (2023) Direct evidence of helium rain in Jupiter and Saturn. arxiv: 2310:13412
- Christensen U, Wicht J, , et al (2020) Mechanisms for Limiting the Depth of Zonal Winds in the Gas Giant Planets. *ApJ* 890:61
- Cohen I, Beddingfield C, Chanca R, et al (2022) The Case for a New Frontiers-Class Uranus Orbiter: System Science at an Underexplored and Unique World with a Mid-scale Mission. *PSJ* 3:58. <https://doi.org/10.3847/PSJ/ac5113>
- Conrath B, Gautier D (2000) Saturn helium abundance: A reanalysis of voyager measurements. *Icarus* 144:124
- Conrath B, Gautier D, R.A. H, et al (1984) The Helium Abundance of Saturn from Voyager Measurements. *ApJ* 282:807–815
- Conrath B, Gautier D, Hanel R, et al (1987) The Helium Abundance of Uranus from Voyager Measurements. *JGR* 92:15,003–15,010
- Conrath B, Gautier D, Lindal G, et al (1991) The Helium Abundance of Neptune from Voyager Measurements. *JGRS* 96:18,907–18,919
- Debras F, Chabrier G (2019) New Models of Jupiter in the Context of Juno and Galileo. *ApJ* 872:100
- Desjarlais M (2003) Density-functional calculations of the liquid deuterium Hugoniot, reshock, and reverberation timing. *PRB* 68:064204. <https://doi.org/10.1103/PhysRevB.68.064204>
- Fortney J, Hubbard W (2003) Phase Separation in Giant Planets: Inhomogeneous evolution of Saturn. *Icarus* 164:228
- Fortney J, Militzer CB, Mankovich, Helled R, et al (2023) Saturn’s Interior After the Cassini Grand Finale. arXiv e-prints <https://doi.org/10.48550/arXiv.2304.09215>

- Gautier D, Conrath B, Flasar M, et al (1981) The Helium Abundance of Jupiter from Voyager. *JGR* 86:8713–8720
- Goncharov A (2020) Phase diagram of hydrogen at extreme pressures and temperatures; updated through 2019 (Review article). *Low Temperature Physics* 46:97–103. <https://doi.org/10.1063/10.0000526>
- Guillot T, Hueso R (2006) The composition of Jupiter: sign of a (relatively) late formation in a chemically evolved protosolar disc. *MNRAS* 367:L47
- Guillot T, Chabrier G, Morel P, et al (1994) Nonadiabatic Models of Jupiter and Saturn. *Icarus* 112:354
- Guillot T, Li C, Bolton S, et al (2020) Storms and the depletion of ammonia in Jupiter: II. Explaining the Juno observations. *JGR: Planets* 125:e2020JE006404
- Gupta P, Atreya S, Steffes P, et al (2022) Jupiter’s Temperature Structure: A Reassessment of the Voyager Radio Occultation Measurements. *PSJ* 3:159
- Helled R, Fortney J (2020) The Interiors of Uranus and Neptune: Current Understanding and Open Questions. *Phil Trans R Soc A* 378:20199474
- Helled R, Anderson J, Podolak M, et al (2011) Interior models of Uranus and Neptune. *ApJ* 726:A15
- Helled R, Mazzola G, Redmer R (2020) Understanding dense hydrogen at planetary conditions. *Nature Reviews Physics* 2:562–574. <https://doi.org/10.1038/s42254-020-0223-3>
- Helled R, Nettelmann N, Guillot T (2020) Uranus and Neptune: origin, evolution and internal structure. *SSRv* 216:38
- Horn H, Prakapenka V, Chariton S, et al (2023) Reaction between Hydrogen and Ferrous/Ferric Oxides at High Pressures and High Temperatures—Implications for Sub-Neptunes and Super-Earths. *PSJ* 4:30
- Howard S, Guillot T (2023) Accounting for non-ideal mixing effects in the hydrogen-helium equation of state. *A&A* 672:L1. <https://doi.org/10.1051/0004-6361/202244851>
- Howard S, Guillot T, Bazot M, et al (2023) Jupiter’s interior from Juno: Equation-of-state uncertainties and dilute core extent. *A&A* 672:A33. <https://doi.org/10.1051/0004-6361/202245625>
- Hsu D, Ford E, Ragozzine D, et al (2019) Occurrence Rates of Planets Orbiting FGK Stars: Combining Kepler DR25, Gaia DR2, and Bayesian Inference. *AJ* 158:109

- Kaspi Y, Showman A, Hubbard W, et al (2013) Atmospheric confinement of jet streams on Uranus and Neptune. *Nature* 497:344
- Knudson M, Desjarlais M (2017) High-Precision Shock Wave Measurements of Deuterium. *PRL* 348:1455
- Knudson M, Desjarlais M, Becker A, et al (2015) Direct observation of an abrupt insulator-to-metal transition in dense liquid deuterium. *Science* 118:035501
- Koskinen TT, Guerlet S (2018) Atmospheric structure and helium abundance on Saturn from Cassini/UVIS and CIRS observations. *Icarus* 307:161–171
- Kunimoto M, Matthews J (2020) Searching the entirety of Kepler data. II. Occurrence rate estimates for FGK stars. *AJ* 159:248
- Leconte J, Chabrier G (2013) Layered convection as the origin of Saturn’s luminosity anomaly. *Nature Geo* 6:347
- Lindal G (1992) The atmosphere of Neptune: an analysis of radio occultation data acquired with Voyager 2. *Astronom J* 103:967
- Lorenzen W, Holst B, Redmer R (2009) Demixing of hydrogen and helium at megabar pressures. *PRL* 102:5701
- Lorenzen W, Holst B, Redmer R (2011) Metallization in hydrogen-helium mixtures. *PRB* 84:235109
- Loubere P, LeToullec R, Pinceaux J (1991) Estimating the number of planets that PLATO can detect. *J Phys Condens Matter* 3:3183
- Loubeyre P, Le Toullec R, Pinceaux JP (1987) Binary phase diagrams of H₂-He mixtures at high temperature and high pressure. *PRB* 36:3723–3730. <https://doi.org/10.1103/PhysRevB.36.3723>
- Mandt K (2023) The first dedicated ice giants mission. *Science* 379:640–642. <https://doi.org/10.1126/science.ade8446>
- Mankovich C, Fortney J (2020) Evidence for a Dichotomy in the Interior structures of Jupiter and Saturn rom Helium Phase separation. . *ApJ* 889:51
- Mankovich C, Fuller J (2021) A diffuse core in Saturn revealed by ring seismology. *Nat Ast* 0:accepted
- McMahon J, Morales M, Pierleoni C, et al (2012) The properties of hydrogen and helium under extreme conditions. *Reviews of Modern Physics* 84:1607–1653. <https://doi.org/10.1103/RevModPhys.84.1607>

- Miguel Y, Bazot M, Guillot T, et al (2022) Jupiter’s inhomogeneous envelope. *A&A* 662:A18. <https://doi.org/10.1051/0004-6361/202243207>
- Militzer B, Hubbard WB (2013) An initio eos for h-he mixtures with recalibration of the giant planet m-r relationship. *ApJ* 774:148
- Militzer B, Hubbard WB (2023) Relation of Gravity, Winds, and the Moment of Inertia of Jupiter and Saturn. *PSJ* 4:95. <https://doi.org/10.3847/PSJ/acd2cd>
- Militzer B, Wahl S, Hubbard W (2019) Models of Saturn’s Interior Constructed with an Accelerated Concentric Maclaurin Spheroid Method. *ApJ* 879:78
- Moore K, Barik A, Stanley S, et al (2022) Dynamo simulations of Jupiter’s magnetic field: The role of stable stratification and a dilute core. *JGR:Planets* 127:e2022JE007479
- Morales MA, Hamel S, Caspersen K, et al (2013) Hydrogen-helium demixing from first-principles: from diamond anvil cells to planetary interiors. *PRB* 87:174105
- Movshovitz N, Fortney J (2022) The Promise and Limitations of Precision Gravity: Application to the Interior Structure of Uranus and Neptune. *PSJ* 3:88
- Nettelmann N, Helled R, Fortney J, et al (2013) New indication for a dichotomy in the interior structure of Uranus and Neptune from the application of modified shape and rotation data. *Planet Sp Sci* 77:143–151
- Nettelmann N, Fortney JJ, Moore K, et al (2015) An exploration of double diffusive convection in jupiter as a result of hydrogen-helium phase separation. *MNRAS* 447:3422
- Nettelmann N, Wang K, Fortney J, et al (2016) Uranus evolution models with simple thermal boundary layers. *Icarus* 275:107
- Nettelmann N, Movshovitz N, Ni D, et al (2021) Theory of Figures to the Seventh Order and the Interiors of Jupiter and Saturn. *PSJ* 2:241. <https://doi.org/10.3847/PSJ/ac390a>
- Neuenschwander B, Helled R (2022) Empirical structure models of Uranus and Neptune. *MNRAS* 512:3124–3136
- Neuenschwander B, Müller S, Helled R (2024) Uranus’ Complex Internal Structure. accepted to *A&A* p arXiv:2401.11769. <https://doi.org/10.48550/arXiv.2401.11769>
- Ni D (2020) Understanding Saturn’s interior from the Cassini Grand Finale gravity measurements. *A&A* 639:A10
- Niemann H, Atreya S, Carignan G, et al (1998) The composition of the Jovian atmosphere as determined by the Galileo probe mass spectrometer. *JGR* 103:831–845

- Orton G, Ingersoll A (1980) Saturn's Atmospheric Temperature Structure and Heat Budget. *JGR* 85:5871
- Podolak M, Helled R, Schubert G (2019) Effect of non-adiabatic thermal profiles on the inferred compositions of Uranus and Neptune. *MNRAS* 487:2653–2664
- Preising M, Redmer R (2019) High-pressure melting line of helium from ab initio calculations. *PRB* 100:184107
- Redmer R, Mattsson TR, Nettelmann N, et al (2011) The phase diagram of water and the magnetic field of Uranus and Neptune. *Icarus* 211:798–803
- Salaheddine C, Théveneau P, Coquelet C, et al (2020) Measurements and predictive models of high-pressure H₂ solubility in brine (H₂O+NaCl) for underground hydrogen storage application. *Intern J of Hydrogen Energy* 45:32206–32220
- Scheibe L, Nettelmann N, Redmer R (2019) Thermal evolution of Uranus and Neptune I. Adiabatic models. *A&A* 632:A70
- Scheibe L, Nettelmann N, Redmer R (2021) Thermal evolution of Uranus and Neptune II. Deep thermal boundary layer. *A&A* 650:A200
- Schöttler M, Redmer R (2018) Ab Initio Calculation of the Miscibility Diagram for Hydrogen-Helium Mixtures. *PRL* 120:115703
- Schouten J, de Kijper A, Michels J (1991) Critical line of He-H₂ up to 2500 K and the influence of attraction on fluid-fluid separation. *PRB* 44:6630–6634. <https://doi.org/10.1103/PhysRevB.44.6630>
- Sromovsky L, Fry P, Kim J (2011) Methane on Uranus: The case for a compact CH₄ cloud layer at low latitudes and a severe CH₄ depletion at high-latitudes based on re-analysis of Voyager occultation measurements and STIS spectroscopy. *Icarus* 215:292–312
- Stevenson D (1998) States of matter in massive planets. *JPhysCondensMatter* 10:11227
- Stevenson DJ, Salpeter EE (1977a) The dynamics and helium distribution in hydrogen-helium fluid planets. *ApJS* 35:239–261
- Stevenson DJ, Salpeter EE (1977b) The phase diagram and transport properties for hydrogen-helium fluid planets. *ApJS* 35:221–237
- Thorngren D, Fortney J, Murray-Clay R, et al (2016) The Mass-Metallicity relation for giant planets. *ApJ* 831:64
- Tsiganis K, Gomes R, Morbidelli A, et al (2005) Origin of the orbital architecture of the giant planets of the Solar System. *Nature* 435:26

- Vazan A, Helled R (2020) Explaining the low luminosity of Uranus: a self-consistent thermal and structural evolution. *A&A* 633:A50
- Vazan A, Helled R, Kovetz A, et al (2015) Convection and Mixing in Giant Planet Evolution. *ApJ* 803:32
- Wahl S, Hubbard W, Militzer B, et al (2017) Comparing Jupiter interior structure models to Juno gravity measurements and the role of a diluted core. *GRL* 44:4649
- Waite J, Perryman R, Perryman M, et al (2018) Chemical interactions between Saturn's atmosphere and its rings. *Science* 362:0
- Wulff PN, Dietrich W, Christensen UR, et al (2022) Zonal winds in the gas planets driven by convection above a stably stratified layer. *MNRAS* 517:5584–5593. <https://doi.org/10.1093/mnras/stac3045>
- Zaghoo M, Salamat A, Silvera I (2016) Evidence of a first-order phase transition to metallic hydrogen. *PRB* 15:155128
- von Zahn U, Hunten DM, Lehmacher G (1998) Helium in jupiter's atmosphere: Results from the galileo probe helium interferometer experiment. *JGR* 103:22815